Electronic Supplementary Material (ESI) for Journal of Materials Chemistry A.
This journal is © The Royal Society of Chemistry 2021

Supporting Information

Toward High-temperature Thermal Tolerance in Solar Selective Absorber Coatings: Choosing High Entropy Ceramics HfNbTaTiZrN

Cheng-Yu He[a], Xiang-Hu Gao[a,b*], Dong-Mei Yu[a], Shuai-Sheng Zhao[a], Hui-Xia Guo[c*], Gang Liu[a,b*]

[a] *Research and Development Center for Eco-Chemistry and Eco-Materials, State Key Laboratory of Solid Lubrication, Lanzhou Institute of Chemical Physics, Chinese Academy of Sciences, Lanzhou 730000, China*

[b] *Center of Materials Science and Optoelectronics Engineering, University of Chinese Academy of Sciences, Beijing 100049, China*

[c] *Key Laboratory of Bioelectrochemistry & Environmental Analysis of Gansu Province, College of Chemistry & Chemical Engineering, Northwest Normal University, Lanzhou 730070, China*

* Corresponding author:
E-mail address: gaoxh@licp.cas.cn (Xiang-Hu Gao)
guohx@nwnu.edu.cn (Hui-Xia Guo)
gangliu@licp.cas.cn (Gang Liu)

Supplementary Note 1: Optical models

$$\varepsilon_{HMVF} = \varepsilon_{back\ ground} + \varepsilon_{Drude} + \Sigma\varepsilon_{Kim} + \varepsilon_{OJL} \quad \text{(S1)}$$

In the case of doped semiconductors the charge carriers set free by the donors or acceptors can be accelerated by very little energies and hence do respond to applied electric fields with frequencies in the infrared region, which is given by the Drude model[1-3].

$$\varepsilon_{LMVF} = \varepsilon_{back\ ground} + \Sigma\varepsilon_{Kim} + \varepsilon_{OJL} \quad \text{(S2)}$$

The OJL model is used to show interband transitions put forward by OLeary model where expressions for the joint density of states are given for optical transition from the valence band to the conduction band[4-5].

Table S1 Deposition and fitting parameters of HfNbTaTiZrN varying N_2 flow rate from 1 to 5 sccm.

Samples	N_2 (sccm)	O_2 (sccm)	Deposited Time (min)	RF power (W)	Thickness (nm)	Deviation value
HfNbTaTiZrN	1	0	20	200	140	0.0000219
	2	0	20	200	140	0.0000735
	3	0	20	200	136	0.0000207
	4	0	20	200	136	0.0000193
	5	0	20	200	132	0.0000419

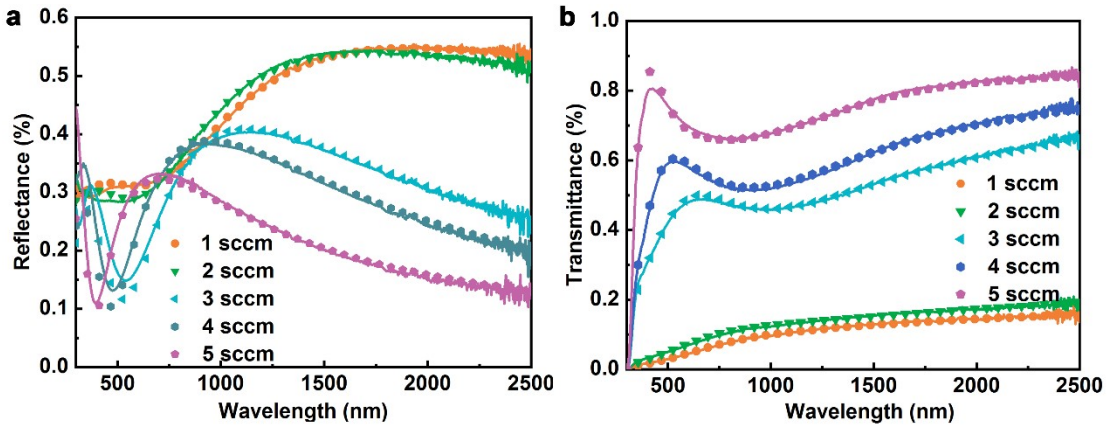

Fig. S1. The measured and simulated (a) T and (b) R spectra of HfNbTaTiZrN coatings on glass substrates varying N_2 flow rate from 1 to 5 sccm.

Supplementary Note 2: Experimental details

2.1The deposition process of the coatings

The HfNbTaTiZrN (HMVF)/HfNbTaTiZrN (LMVF)/SiO_2 SSACs were deposited on (SS) substrates (model 304, dimensions 50 mm × 50 mm) through a reactive DC/RF magnetron sputtering system (Kurt J. Lesker, USA) that has constant target current. The substrate bias keeps constant and substrate temperature does not change in room temperature. Prior to be placed into the vacuum chamber, all substrates were cleaned with alcohol, acetone and de-ionized water in an ultrasonic agitator. The base pressure was pumped down to 5.0×10^{-6} mtorr by a cryopump. An immensely pure HEA HfNbTaTiZr target (purity 99.9%) was used to fabricate HMVF layer and LMVF layer, which is carried out in an Ar/N_2 atmosphere. With aid of the mixed Ar/O_2 atmosphere, the SiO_2 layer was fabricated on top of LMVF layer. The thickness of those films was controlled by the method that calculate the film grow rate by means of deposition time.

2.2 Characterization

The reflectance spectra of the SS/HMVF/LMVF/SiO_2 coatings in solar spectrum range (0.3-2.5 μm) were obtained by a Perkin Elmer Lambda 950 UV/Vis/NIR Spectrometer with an integration sphere (module 150 mm) and reflectance spectra in the infrared region (2.5-25 μm) were measured on a Bruker TENSOR 27 FT-IR Spectrometer, equipped with an integrating sphere (A562-G/Q) using a gold plate as a standard for diffuse reflectance. According to experimental spectra, and the normal α_s and ε_T values were obtained by Eqs. (S3) and (S4).

$$\alpha_S = \frac{\int_{0.3\mu m}^{2.5\mu m} \left[1 - R(\lambda)\right] I_{sol}(\lambda) d\lambda}{\int_{0.3\mu m}^{2.5\mu m} I_{sol}(\lambda) d\lambda} \tag{S3}$$

where λ is the specific wavelength, $R(\lambda)$ presents reflectance and $I_{sol}(\lambda)$ is the direct normal solar irradiance which is defined according to ISO standard 9845-1, normal radiance, AM 1.5. Normal thermal emittance ε_T is equally a weighted fraction but between emitted radiation and the Planck black body distribution, $I_b(\lambda, T)$, at temperature T.

$$\varepsilon_{\mathrm{T}} = \frac{\int_{2.5\mu m}^{25\mu m}\left[1-R(\lambda)\right] I_b(\lambda,T)\,d\lambda}{\int_{2.5\mu m}^{25\mu m} I_b(\lambda,T)\,d\lambda} \tag{S4}$$

It is worth to note that the reflectance spectra of the absorbers before and after annealing were measured at 82 °C. Accordingly, solar absorptance and thermal emittance of the absorbers at high temperatures were calculated based on the reflectance spectra. Given that optical properties of absorber are closely related to working temperatures, an optical simulation is carried out to estimate the emittance based on reported dependence for SS substrate. The simulation results indicate that the thermal emittance is underestimated by 3-4% (**Fig. S9**).

Based on the measured spectra (reflectance and transmittance) of HMVF and LMVF film deposited on glass, CODE software is utilized to calculate the optical constants (n, k) by fitting the experimental transmittance and reflectance spectra. X-ray diffraction (XRD) patterns were recorded on a Rigaku D/max 2400/PC diffractometer (Rigaku Corporation, Tokyo, Japan) with Cu Ka radiation (l51.5406 Å). The surface morphologies were observed by ultra-high resolution scanning electron microscope (SU8200, Tokyo, Japan) and high-resolution transmission electron microscopy (TEM, JEOL JEM-2100F). The Raman spectra were obtained using a Raman technique (LabRAM HR Evolution, HORIBA).

One of the most significant features of semiconductor materials is the energy gap (E_g) that determines solar absorption. Herein, the energy gap of HfNbTaTiZrN films deposited with different N_2 flow rates were estimated by Tauc formula as below:

$$(\alpha^0 hv)^n = K(hv - E_g) \tag{S5}$$

where hv is the photon energy, E_g represents the optical bandgap of the involved

materials, and K represents the energy-independent constant, absorption coefficient (α^0) of the HfNbTaTiZrN films at different wavelengths are obtained from the reflectance spectra. In addition, n = 2 for direct bandgap transitions, and n = ½ for indirect transitions. The values of the bandgap energy are calculated by extrapolating the linear fitted region at $(\alpha^0 hv)^n$ versus the photon energy (hv).

Table S2 The detailed deposition parameters of individual layers.

Layer	RF power (W)	N_2 (sccm)	O_2 (sccm)	Thickness (nm)	Deposited time (min)	Absorbance (α)	Emittance (ε)
HMVF	200	2	0	52	8	73.6%	7%
LMVF	200	5	0	46	20	85.8%	7%
SiO_2	160	0	8	151	280	96.0%	8.2%

Supplementary Note 3: Elemental analysis and thermodynamics of HfNbTaTiZr target and HfNbTaTiZrN coatings

Table S3 Elemental analysis of HfNbTaTiZr target.

Element	Hf	Nb	Ta	Ti	Zr
Radius (Å)	1.59	1.46	1.46	1.47	1.60
Structure	hcp	bcc	bcc	hcp	hcp
Melting point (ºC)	2233	2477	3017	1668	1855

Table S4 The EDS analysis of HfNbTaTiZr target.

Element	Hf	Nb	Ta	Ti	Zr
Content (at%)	22.59	17.36	17.19	20.82	22.04

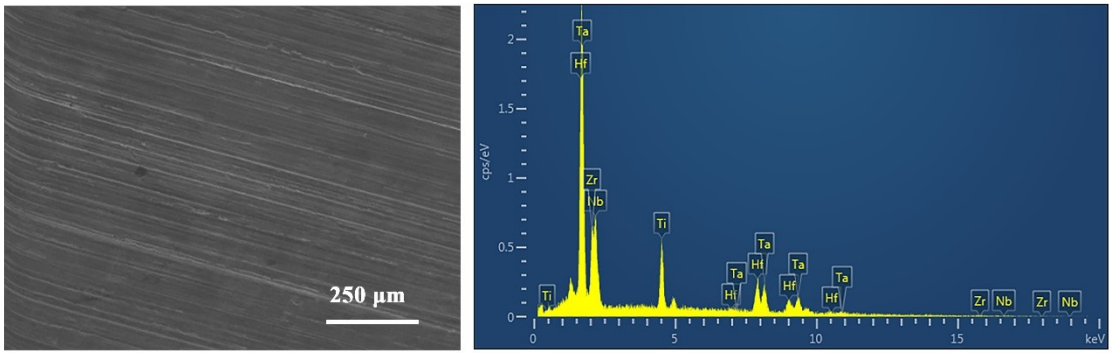

Fig. S2. The EDS analysis of HfNbTaTiZr target.

Table S5 EDS analysis of HMVF layer

N_2 flow rate	Hf	Nb	Ta	Ti	Zr	N
2 sccm	10.14	14.74	11.93	12.78	14.73	35.69
5 sccm	8.66	11.36	9.49	10.08	11.15	49.27

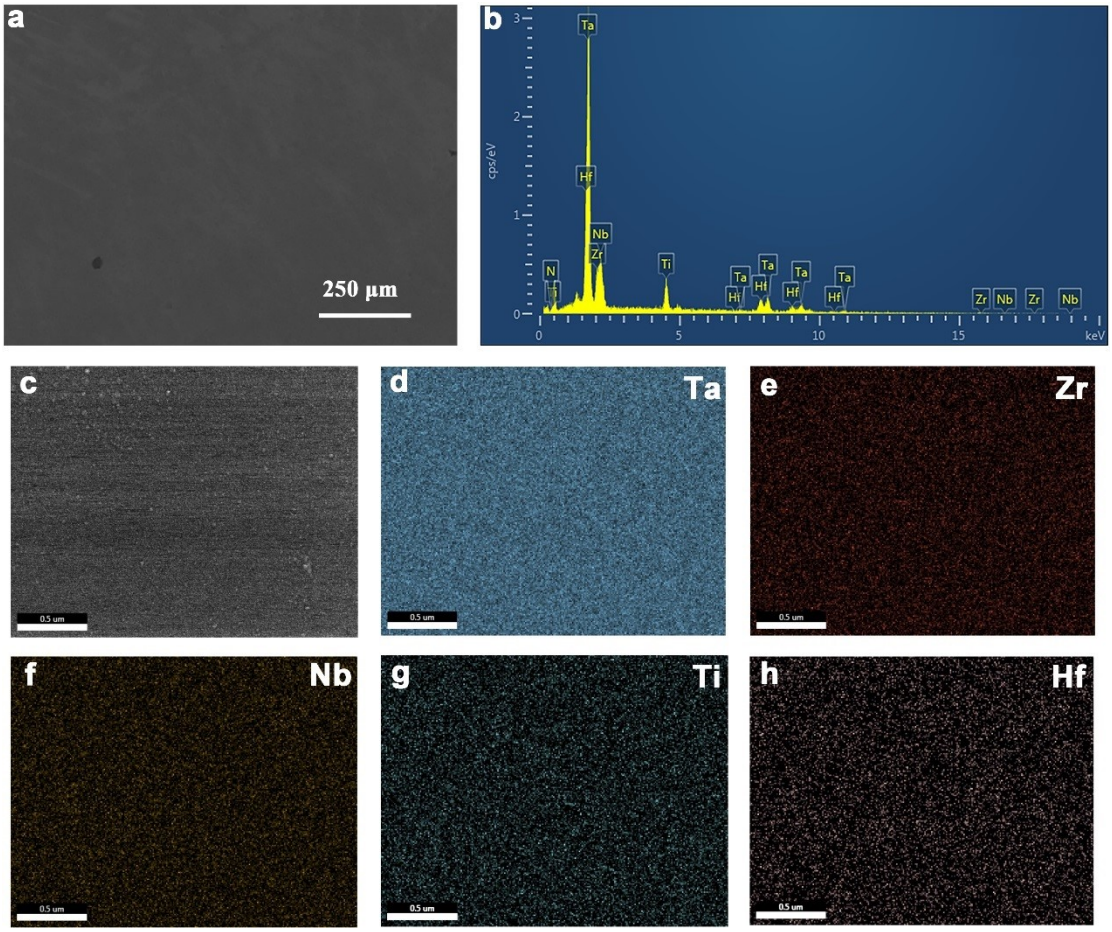

Fig. S3. EDS analysis of HMVF layer.

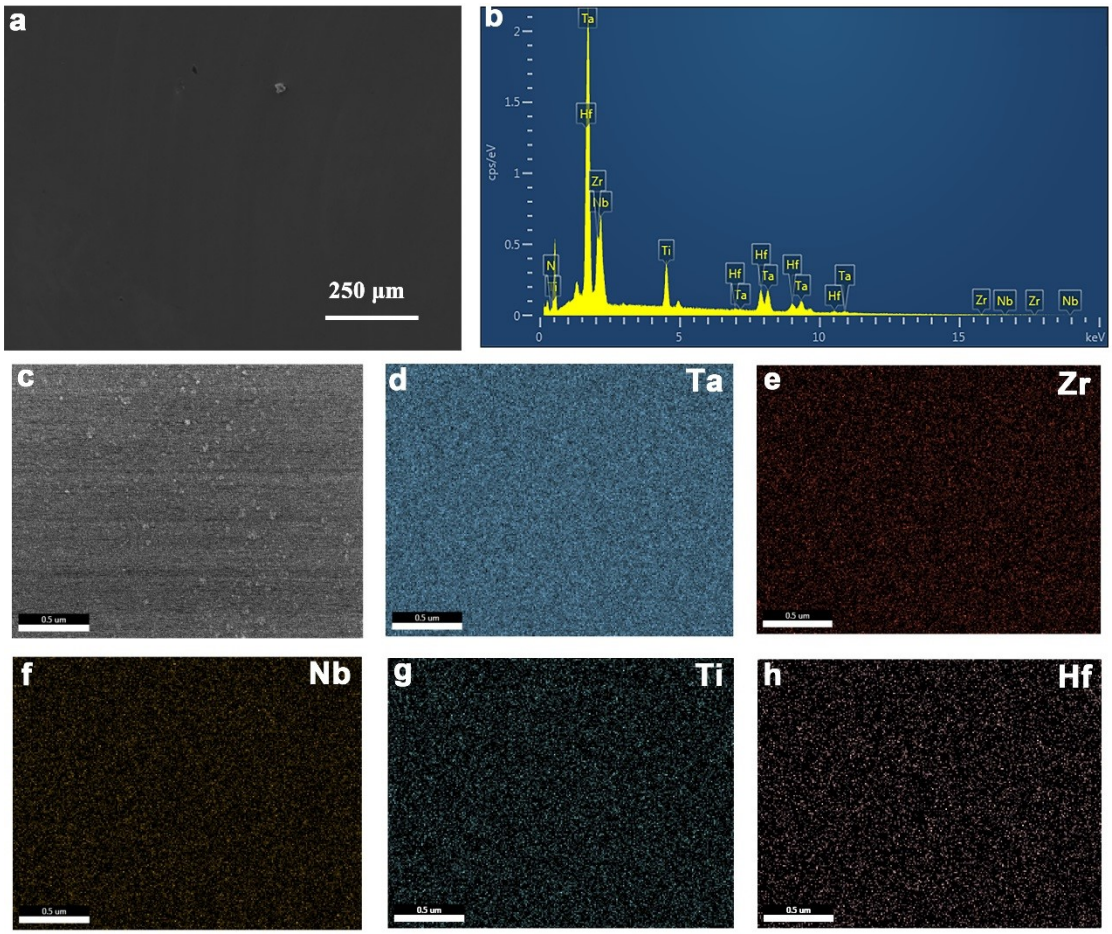

Fig. S4. EDS analysis of LMVF layer.

To judge whether the coating meets the definition of high entropy alloy, we extensively investigate elemental contents in HfNbTaTiZr target and HfNbTaTiZrN coatings. The radius, structure and melting point of involved elements are list in **Table S3.** Note that the sizes of target elements are very close, which increase the mutual solid solution property. The element contents in HfNbTaTiZr target are measured, which is shown in **Fig. S2** and **Table S4**. The atomic percentages of the involved elements are very close to 1:1:1:1:1. The EDS analyses of HMVF and LMVF layer are carried out **(Fig. S3 and S4, Table S5**), in which approximate equimolar ratio can be seen with the except of nitrogen element. According to Boltzmann's hypothesi[6-8], the entropy of mixing in multi-principal elements alloy HfNbTaTiZr is obtained:

$$\Delta S_{mix} = -R\sum_{i=1}^{n}(c_i \ln c_i) \quad \text{(S6)}$$

c_i is mole percent of component, and R (=8.314 J K^{-1} mol^{-1}) is gas constant. According to equation (S6), the ΔS_{mix} of multi-principal elements alloy HfNbTaTiZr is calculated to be 1.6R. We can hence conclude that HfNbTaTiZr alloy is high entropy alloy.

To predict the solid-solution formation rule in high entropy alloy HfNbTaTiZr, we first consider the Gibbs free energy of multi-component system. The ΔG_{mix} can be expressed as:

$$\Delta G_{mix} = \Delta H_{mix} - T\Delta S_{mix} \quad \text{(S7)}$$

where T represents the absolute temperature, ΔH_{mix} represents the enthalpy of mixing and ΔS_{mix} represents the entropy of mixing. To simplify the calculation for free

energy, the enthalpy of mixing for high entropy alloy HfNbTaTiZr with five elements can be obtained as below :

$$\Delta H_{mix} = \ - R \sum_{i=1, i \neq j}^{n} \Omega \, c_i c_j \tag{S8}$$

A parameter Ω is used to predict the formation of solid-solution, as shown in below:

$$\Omega = \frac{T_m \Delta S_{mix}}{|\Delta H_{mix}|} \tag{S9}$$

Where melting temperature (T_m) of the high entropy alloy signifies the phase formation, which can be expressed as follows:

$$T_m = \sum_{i=1}^{n} c_i (T_m)_i \tag{S10}$$

Considering the atomic size mismatch effect of component atoms, the parameter of is introduced:

$$\delta = \sqrt{\sum_{i=1}^{n} c_i (1 - \frac{r_i}{\bar{r}})^2} \tag{S11}$$

The combination of parameters Ω and δ, should be proposed as a criterion for forming solid-solution phase. According to the result calculated above, high entropy alloy HfNbTaTiZr is attributed to solid solutions (**Fig. S5)**.

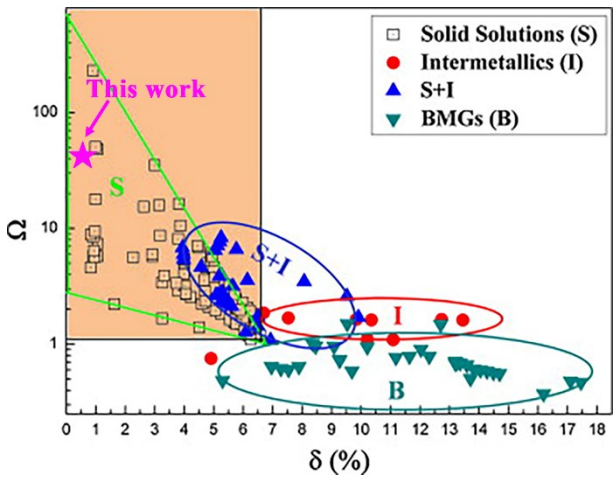

Fig. S5. The relationship between parameters **Ω** and δ .

Table S6 The binary mixing enthalpy between elements in multi-element films ΔH_{AB}^{mix} kJ/mol.

	Hf	Nb	Ta	Ti	Zr
Hf					
Nb	4				
Ta	3	0			
Ti	0	2	1		
Zr	0	4	3	0	
N	-218	-174	-173	-190	-233

Table S7 The thermodynamic parameters of HEA HfNbTaTiZr.

	ΔH_{mix} (kJ/mol)	ΔS_{mix} (J/K)	T_m (K)	δ %	Ω
HfNbTaTiZr	0.592577	13.325325	2482.1828	0.0435706644	55.8170373123

Supplementary Note 4: simulation on the electromagnetic wave propagation

A commercial finite-difference time-domain (FDTD) software package Lumerical Solution are employed to simulate the light propagation[9-11]. A plane wave from +z towards -z direction is selected to be incident light source. The model geometry is devised according to the schematic drawing of SSAC displayed in **Fig. 1b**. Periodic boundary conditions are used to model x and y direction, perfectly matched layer (PML) is for z direction. The mesh element size of $2\times2\times1$ nm^3 is utilized to improve simulation accuracy. Absorption power distribution is monitored by extracting from the 2-D XZ or YZ plane.

Supplementary Note 5: Investigation on phase structure and elemental distribution

Table S8 The crystal structures and lattice constants of individual nitrides in HfNbTaTiZrN.

Nitride	HfN	NbN	TaN	TiN	ZrN
Crystal structure Crystal spacing (nm)	fcc	fcc	fcc	fcc	fcc
(111)	2.61	2.53	2.50	2.54	2.64
(200)	2.26	2.19	2.17	2.20	2.29
(220)	1.60	1.55	1.54	1.56	1.62

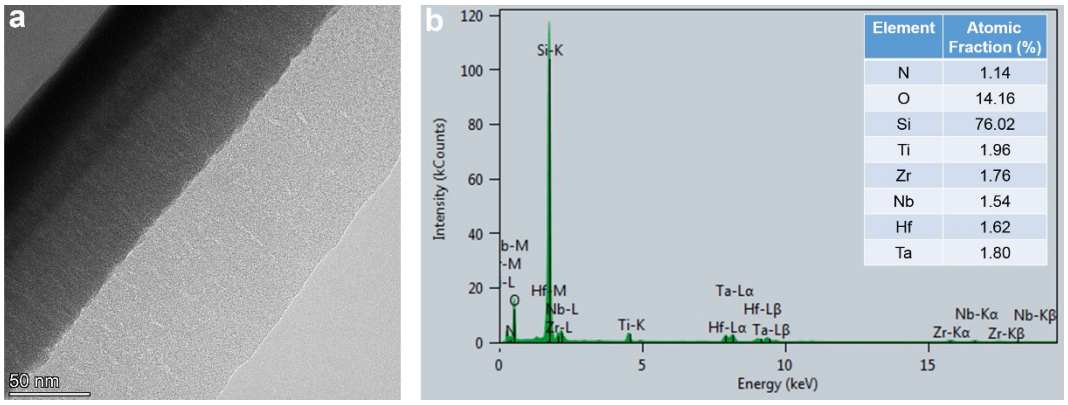

Fig. S6. (a) Scanning TEM image, (c) EDS spectrum of the as-deposited coating.

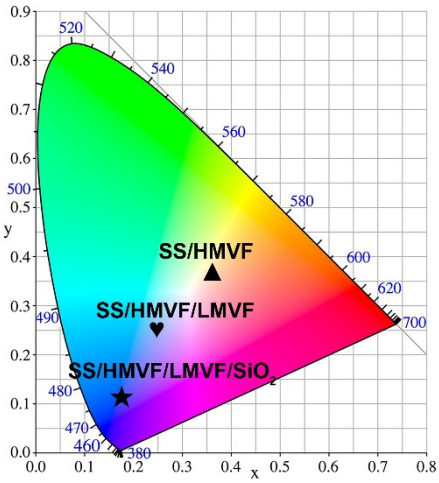

Fig. S7. Chromaticity diagram of the layer-added absorber coatings.

Supplementary Note 6: Evaluation of thermal stability and service life

The performance criteria after annealing treatment of the SSAC are estimated by a performance criterion (PC) function. The PC value shows the influence of heat-treatment tradition on solar absorptance (Δα) and emittance (Δε) of the involved absorber. The PC value requires less than 0.05 corresponding to 5% reduction in the annual solar fraction of solar absorbing coating; the maximum possible service life is determined by the time to reach 0.05 PC value as below;

$$PC = -\Delta\alpha + 0.5\Delta\varepsilon \leq 0.05 \quad \text{(S12)}$$

where Δα = α (after annealing treatment) – α (pristine), Δε = ε (after annealing treatment) – ε (pristine). The PC values are calculated in annealing treatment for preliminary assessment of high temperature thermal stability of our proposed high entropy alloy nitride based SSAC.

It is reported that the slope of natural logarithm of time for PC attaining 0.05 vs working temperature (K^{-1}) is proportional to the activation energy for optical degradation[12]. The time using to reach PC=0.05 can be estimated as listed in **Table 9.** As shown in **Fig. S8a**, the slope is calculated to 33439.51 which corresponds to E_a/R, wherein the R equals to 8.314 $Jmol^{-1}K^{-1}$ is the universal gas constant. The activation energy (E_a) is therefore calculated to be 278 kJ/mol, which is used to measure theoretical lifetime of the proposed SSAC according to Arrhenius equation as follows:

$$\ln\left(\frac{t_{(test)}}{t_{(ref)}}\right) = -\frac{E_a}{R}\left(\frac{1}{T_{ref}} - \frac{1}{T_{test}}\right) \quad \text{(S13)}$$

where $T_{(test)}$ is the test temperature, $T_{(ref)}$ is reference temperature, $t_{(ref)}$ is life time (PC = 0.05) at reference temperature, t (test) is life time (PC=0.05) at test temperature. Based the calculated activation energy, the maximum working time at different temperature can be obtained. Presuming the SSAC will operate 8 h every day, it demonstrates that the maximum temperature corresponding to a service life of ~25 years (73000 hours) and PC = 0.05 is calculated to be 529 °C (**Fig. S8b**). Further on, when the coating works at 500 °C, the serve life could reach up to 124 years.

Table S9 The periods using to reach PC=0.05 at different working temperatures.

Working temperature	700 °C	750 °C	800 °C
Time	50 h	15h	2h

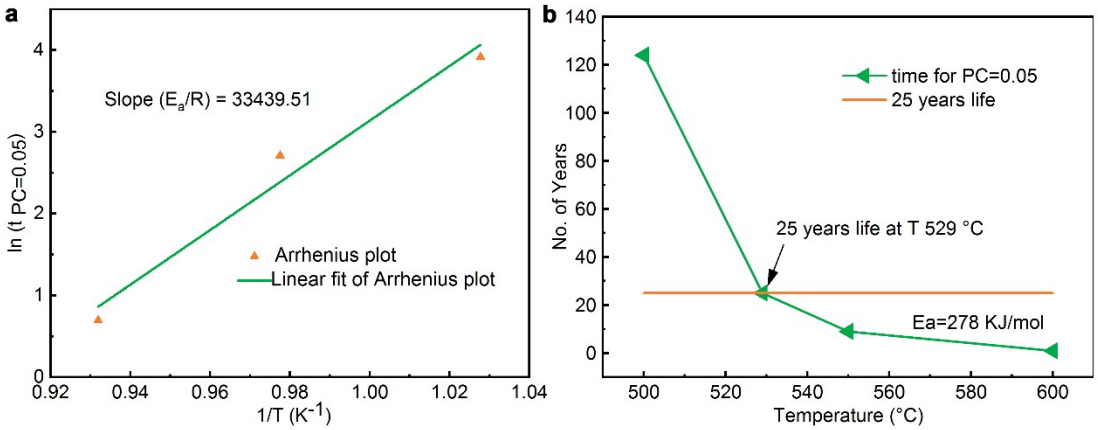

Fig. S8. (a) The relationship between Arrhenius plot of ln ($t_{PC = 0.05}$) and 1/T, the slope is used to determine activation energy (E_a); (b) Evaluation of service lifetime at different working temperatures.

Table S10 Thermal emittance at different working temperatures for the as-deposited SSAC and the sample annealed at 600 °C for 168 h.

Samples	82°C	400°C	500°C	550°C	600°C
As-deposited	8.2%	16.9%	20.6%	22.5%	24.5%
550°C-168 h	7%	14.3%	17.6%	19.4%	21.3%
600°C-168 h	8%	18.1%	22.7%	25.2%	27.8%

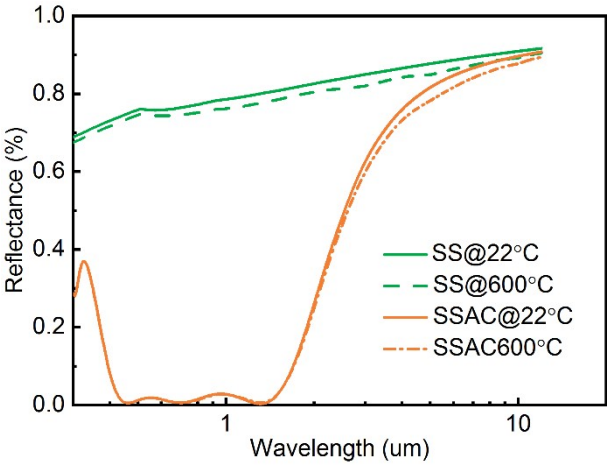

Fig. S9. Reflectance spectra of SS substrate and the HfNbTaTiZrN based SSAC calculated through the optical properties at 22 and 600 °C obtained from previous literature[13].

Table S11 Optical properties, thermal robustness and photothermal conversion efficiency of a series of recently reported state-of-the-art absorbers.

Journal	Material & Class	α	ε	Thermal stability	Ref.
Nat. Energy	Commercial SSA	95%	5%@100°C	500°C vacuum	14
Nano Energy	WTi-Al_2O_3 cermet	93%	10%@500°C	600°C vacuum	15
Adv. Energy mater.	Ta photonic crystal	81%	27%@727°C	727°C vacuum	16
Adv. Mater.	Ni photonic crystal	90%	5%@100°C	800°C vacuum	17
J. Alloy. Compd.	TiN/TiN_xO_y/SiO_2	95.20%	5.4%@80°C	400°C air	18
ACS Appl. Mater. Inter.	AgAl-Al_2O_3 cermet	94.2%	15%@400°C	450°C N_2	19
Appl. Phys. Lett.	Ni-Al_2O_3 cermet	93%	9%@400°C	400°C N_2	20
Appl. Surf. Sci.	TiAlON films	93.6%	17%@82°C	550°C vacuum	21
Adv. Energy Mater.	W-Ni-Al_2O_3 cermet	90%	15%@500°C	600°C vacuum	22
Energy Environ. Sci.	W-Ni-YSZ cermet	91%	13%@500°C	600 °C vacuum	23
J. Materiomics	Mo/ZrSiN/ZrSiON/SiO_2	93.8%	7%@25°C	600°C vacuum	24
Nano Energy	TiN/TiNO/ZrO_2/SiO_2	92.2%	17%@727°C	723°C vacuum	25
Sol. Energy Mater. Sol. Cells	Al/NbMoN/NbMoON/SiO_2	94.8%	5%@80°C	400°C vacuum	26
Sol. Energy Mater. Sol. Cells	HfB_2-ZrB_2/ZrB_2/Al_2O_3	93%	7%@82°C	500°C vacuum	27
Sol. Energy Mater. Sol. Cells	AlCrN/AlCrNO/AlCrN	94%	15%@25°C	500°C air	28
Adv. Mater. Inter.	AgAl-Al_2O_3 cermet	95%	11%@400°C	500°C N_2	29
Nano Energy	$Si_{0.8}Ge_{0.2}$	90%	30%@500°C	750°C air	30
Sol. Energy Mater. Sol. Cells	TiC/Al_2O_3	92%	13%@82°C	650°C vacuum	31
Sol. Energy Mater. Sol. Cells	SiO_2-Si_3N_4-W-SiO_2-W	95%	10%@25°C	400 °C air	32
Sol. RRL	Ti/Al_2O_3/Ta metamaterial	91.3%	24%@727°C	727°C vacuum	33
ACS Appl. Energy Mater.	W/WAlN/WAlON/Al_2O_3	90%	15%@500°C	500 °C vacuum	34
ACS Appl. Energy Mater.	porous Ni	93%	12%@100°C	200°C air	35
Sol. Energy Mater. Sol. Cells	Ni-Al_2O_3	93%	5%@100°C	300°C air	36
J. Mater. Chem. A	Al-AlN_xO_y	94.5%	5.5%@25°C	350 °C air	37
Nat. Commun.	Graphene-based	91%	4%@100°C	100 °C air	38
J. Mater. Chem. A	W-WO_x	93%	5.8%25°C	250 °C air	39
J. Mater. Chem. A	AlCrTaTiZrN	92.8%	15%@600°C	650 °C vacuum	40
Sol. Energy Mater. Sol. Cells	MoNbHfZrTiN	93.5%	9%@82°C	400 °C vacuum	41
This work	HfNbTaTiZrN@Cu	94.8%	4.8%°C	200 °C air	
This work	HfNbTaTiZrN@SS	96%	22%@550°C	600 °C vacuum	

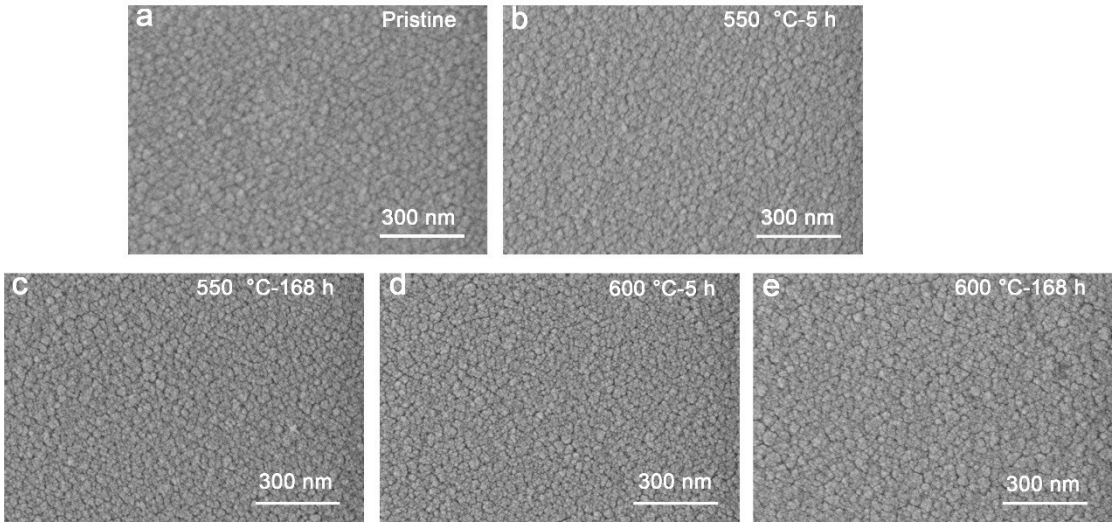

Fig. S10. SEM images of (a) the pristine coating and annealed at 550 °C for (b) 5 h and (c) 168 h, at 600 °C for (d) 5 h and (e) 168 h

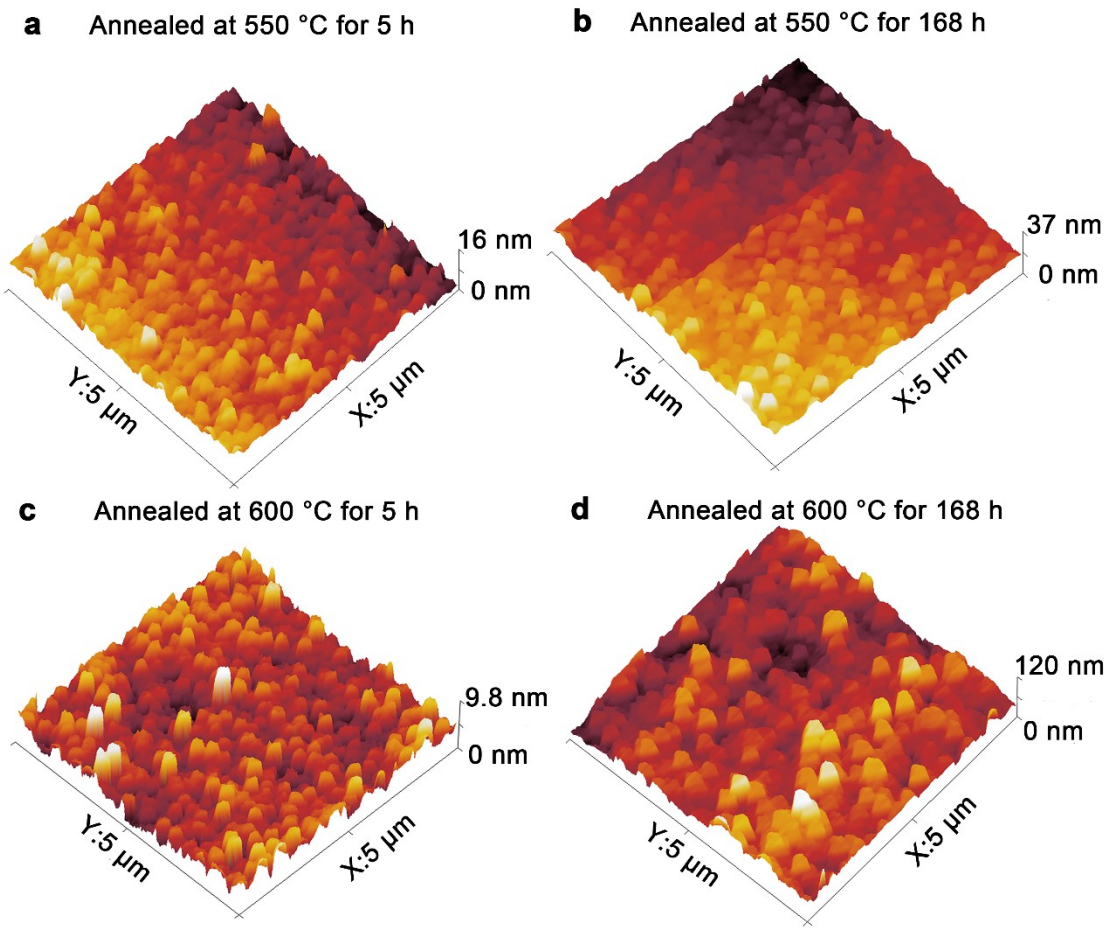

Fig. S11. 3D-AFM images of the coating annealed at 550 °C for (a) 5 h and (b) 168 h, at 600 °C for (c) 5 h and (d) 168 h

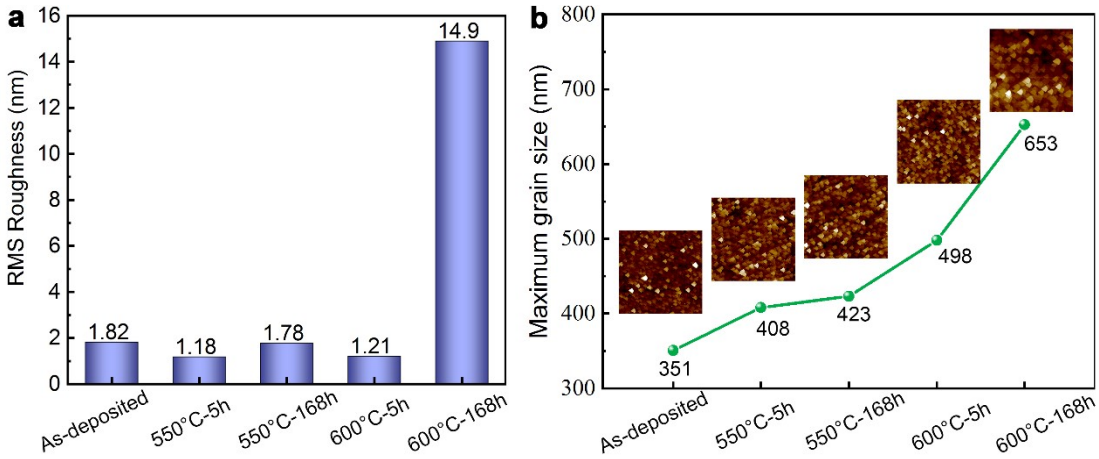

Fig. S12. (a)The RMS roughness and (b) maximum grain sizes of the coating before and after annealing at different temperatures for different times; inset shows corresponding 2-D AFM images.

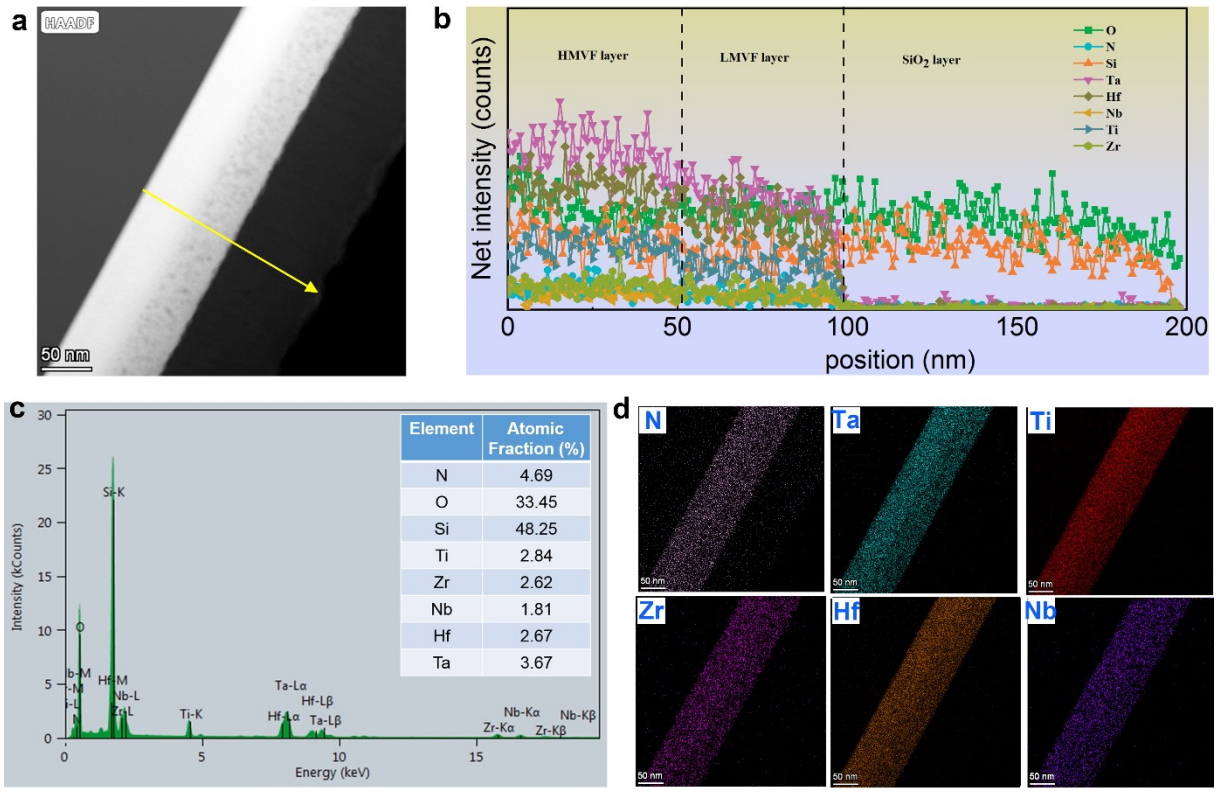

Fig. S13. (a) The scanning TEM image, (b) profile of elements contents and (c) TEM-EDS spectrum of coating after annealing at 600 °C for 168 h; (d) spatial distribution of Hf, Nb, Ta, Ti, Zr, N elements.

Supplementary Note 6: Versatile and scalable high-entropy alloy nitride-based SSAC.

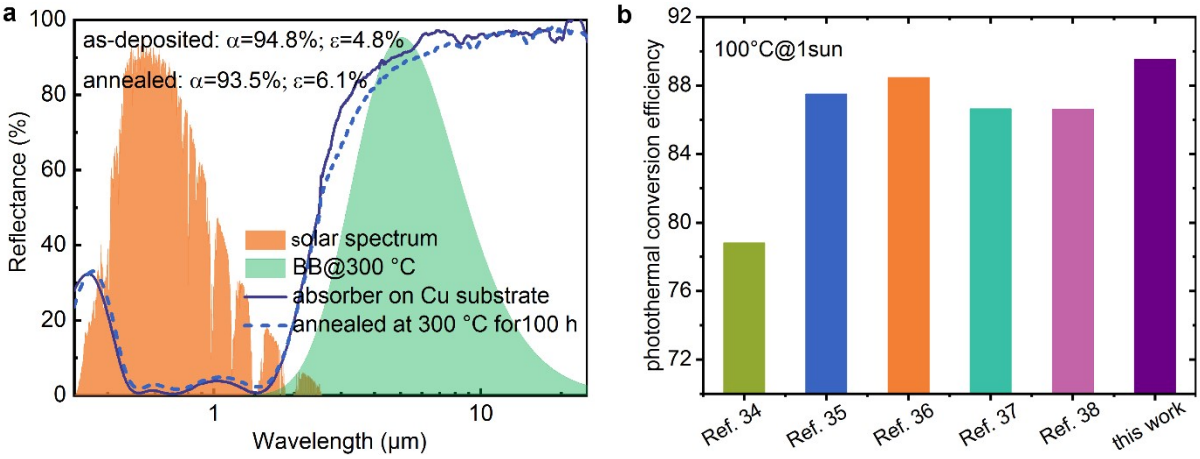

Fig. S14. (a) Reflectance spectra of the SSAC on Cu substrate and the absorber annealed at 300 °C for 100 h; (b) a comparison of photothermal conversion efficiency to recently reported state-of-the-art absorbers used in low temperature.

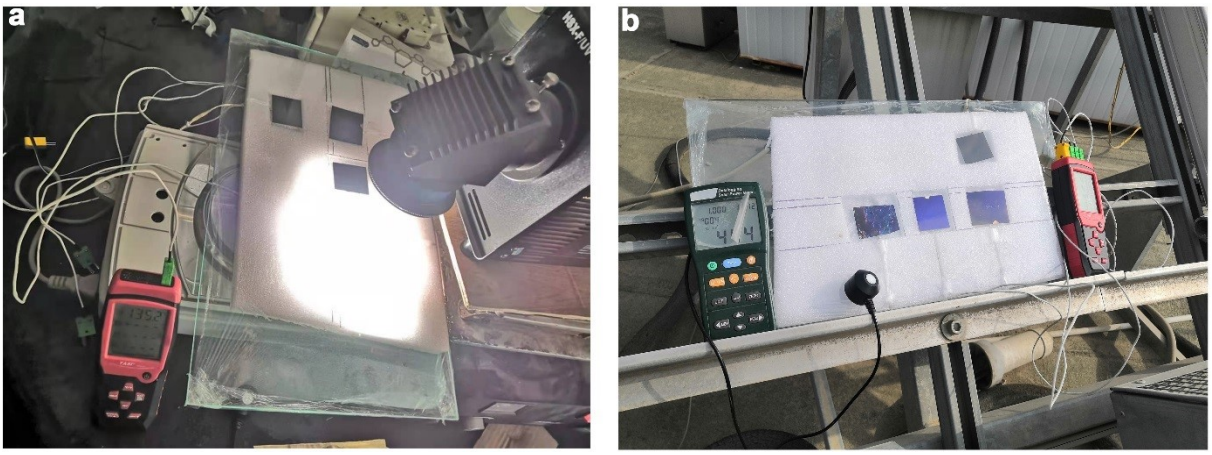

Fig. S15. (a) Indoor and (b) outdoor measures apparatuses.

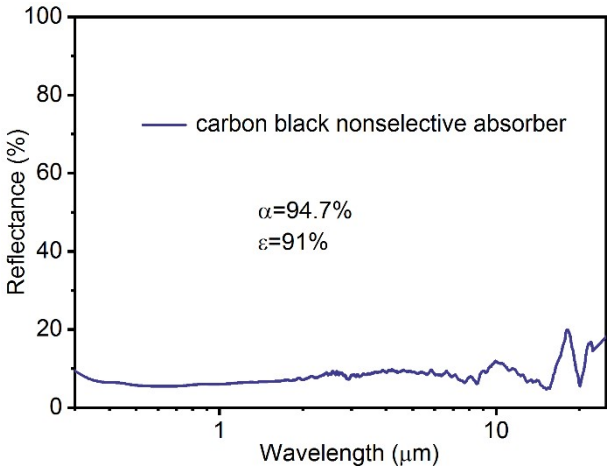

Fig. S16. Reflectance spectrum of a carbon black nonselective absorber.

References:

1. L. Zheng, F. Gao, S. Zhao, F. Zhou, J.P. Nshimiyimana and X. Diao, *Appl. Surf. Sci.*, 2013, **280**, 240-246.

2. L. Rebouta, P. Capela, M. Andritschky, A. Matilainen, P. Santilli, K. Pischow and E. Alves, *Sol. Energy Mater. Sol. Cells*, 2012, **105**, 202-207.

3. S.K. O'Leary, *Solid State Commun.*, 1999, **109**, 589-594

4. Y. Ning, W. Wang, L. Wang, Y. Sun, P. Song, H. Man, Y. Zhang, B. Dai, J. Zhang, C. Wang, Y. Zhang, S. Zhao, E. Tomasella, A. Bousquet and J. Cellier, *Sol. Energy Mater. Sol. Cells*, 2017, **167**, 178-183.

5. X.H. Gao, P.J. Ma, W. Theiss, Y.Q. Shen and G. Liu, *Sol. Energy Mater. Sol. Cells*, 2017, **167**, 150-156.

6. P. Chauhan, S. Chopra and S. Thangaraju, *Adv. Eng. Mater.*, 2019, **21**, 1900251.

7. X. Yang and Y. Zhang, *Mater. Chem. Phys.*, 2012, **132**, 233-238.

8. A. Takeuchi and A. Inoue, *Mater. Trans*. 2005, **46**, 2817-2829.

9. S. Wu, Y. Ye, Z. Jiang, T. Yang and L. Chen, *Adv. Opt. Mater.* 2019, **7**, 1901162.

10. L. Zhou, S. Zhuang, C. He, Y. Tan, Z. Wang and J. Zhu, *Nano Energy*, 2017, **32**, 195-200.

11. G. Shalev, S.W. Schmitt, G. Brönstrup and S. Christiansen, *Nano Energy* 2015, **12**, 801-809.

12. K. Valleti, S. G. Rao, P. Miryalkar, A. Sandeep and D. S. Rao, *Sol. Energy Mater. Sol. Cells*, 2020, **215**, 110634.

13. S. B. Boyden, and Y. Zhang, *J. Thermophys. Heat Tr.*, 2006, **20**, 9-15.

14. G. Ni, G. Li, Svetlana V. Boriskina, H. Li, W. Yang, T. Zhang and G. Chen, *Nat. Energy*, 2016, **1**, 16126.

15. X. Wang, J. Gao, H. Hu, H. Zhang, L. Liang, K. Javaid, F. Zhuge, H. Cao and L. Wang, *Nano Energy*, 2017, **37**, 232-241.

16. V. Rinnerbauer, A. Lenert, D. M. Bierman, Y. X. Yeng, W. R. Chan, R. D. Geil, J. J. Senkevich, J. D. Joannopoulos, E. N. Wang, M. Soljačić and I. Celanovic, *Adv. Energy Mater.*, 2014, **4**, 1400334.

17. P. Li, B. Liu, Y. Ni, K. K. Liew, J. Sze, S. Chen and S. Shen, *Adv. Mater.*, 2015, **27**, 4585-4591.

18. Y. Yang, T. Wang, T. Yao, G. Li, Y. Sun, X. Cao, L. Ma and S. Peng, *J. Alloy. Compd.*, 2020, **815**, 152209.

19. J. Gao, C. Tu, L. Liang, H. Zhang, F. Zhuge, L. Wu, H. Cao and K. Yu, *ACS Appl. Mater. Inter.*, 2014, **6**, 11550-11557.

20. X. Wang, H. Li, X. Yu, X. Shi and J. Liu, *Appl. Phys. Lett.*, 2012, **101**, 203109.

21. H. D. Liu, B. Yang, M. R. Mao, Y. Liu, Y. M. Chen, Y. Cai, D. J. Fu, F. Ren, Q. Wan and X. J. Hu, *Appl. Surf. Sci.*, 2020, **501**, 144025.

22. F. Cao, D. Kraemer, T. Sun, Y. Lan, G. Chen and Z. Ren, *Adv. Energy Mater.*, 2015, **5**, 1401042.

23. F. Cao, D. Kraemer, L. Tang, Y. Li, A. P. Litvinchuk, J. Bao, G. Chen and Z. Ren, *Energy Environ. Sci.*, 2015, **8**, 3040-3048.

24. Y. Ning, C. Wang, W. Wang, E. Tomasella, Y. Sun, P. Song, W. Hao, A. Bousquet, *J. Materiomics*, 2020, **6**, 760-767,

25. Y. Li, C. Lin, D. Zhou, Y. An, D. Li, C. Chi, H. Huang, S. Yang, C. Y. Tso, C. Y. H. Chao and B. Huang, *Nano Energy*, 2019, **64,** 103947.

26. Y. Ning, W. Wang, L. Wang, Y. Sun, P. Song, H. Man, Y. Zhang, B. Dai, J. Zhang, C.

Wang, Y. Zhang, S. Zhao, E. Tomasella, A. Bousquet and J. Cellier, *Sol. Energy Mater. Sol. Cells*, 2017, **167**, 178-183.

27. X.-L. Qiu, X.-H. Gao, C.-Y. He and G. Liu, *Sol. Energy Mater. Sol. Cells*, 2020, **211**, 110533.

28. X. Wang, T. Luo, Q. Li, X. Cheng and K. Li, *Sol. Energy Mater. Sol. Cells*, 2019, **191**, 372-380.

29. J. Gao, X. Wang, B. Yang, C. Tu, L. Liang, H. Zhang, F. Zhuge, H. Cao, Y. Zou, K. Yu, F. Xia and Y. Han, *Adv. Mater. Inter.*, 2016, **3**, 1600248.

30. J. Moon, D. Lu, B. VanSaders, T. K. Kim, S. D. Kong, S. Jin, R. Chen and Z. Liu, *Nano Energy*, 2014, **8**, 238-246.

31. X.-H. Gao, Z.-M. Guo, Q.-F. Geng, P.-J. Ma and G. Liu, *Sol. Energy Mater. Sol. Cells*, 2016, **157**, 543-549.

32. H. Wang, H. Alshehri, H. Su and L. Wang, *Sol. Energy Mater. Sol. Cells*, 2018, **174**, 445-452.

33. Y. Li, D. Li, D. Zhou, C. Chi, S. Yang and B. Huang, *Sol. RRL*, 2018, **2**, 1800057.

34. A. Dan, A. Soum-Glaude, A. Carling-Plaza, C. K. Ho, K. Chattopadhyay, H. C. Barshilia and B. Basu, *ACS Appl. Energy Mater.*, 2019, **2**, 5557-5567.

35. M. Chen, J. Mandal, Q. Ye, A. Li, Q. Cheng, T. Gong, T. Jin, Y. He, N. Yu and Y. Yang, *ACS Appl. Energy Mater.*, 2019, **2**, 6551-6557.

36. Z. Li, J. Zhao and L. Ren, *Sol. Energy Mater. Sol. Cells*, 2012, **105**, 90-95.

37. C. Wang, Z. Li, W. Wang, R. Xia and X. Ling, *J. Mater. Chem. A*, 2019, **7**, 13080-13089.

38. K. T. Lin, H. Lin, T. Yang and B. Jia, *Nat. Commun.*, 2020, **11**, 1389.

39. W. Wang, H. Wen, S. Ling, Z. Li, J. Su and C. Wang, *J. Mater. Chem. A*, 2018, **6**, 15690-

15700.

40. C.-Y. He, X.-H. Gao, D.-M. Yu, X.-L. Qiu, H.-X. Guo and G. Liu, *J. Mater. Chem. A*, 2021, **9**, 6413-6422.

41. C.-Y. He, X.-H. Gao, M. Dong, X.-L. Qiu, J.-H. An, H.-X. Guo and G. Liu, *Sol. Energy Mater. Sol. Cells*, 2020, **217**, 110709.